

A. Kausar^{a,*}, **W. Ullah**^{a,b}, **B. Muhammad**^b, **M. Siddiq**^c

^a *Nanosciences and Catalysis Division, National Centre For Physics, Quaid-i-Azam University Campus, 44000, Islamabad, Pakistan.*

^b *Department of Chemistry, Hazara University, Pakistan.*

^c *Department of Chemistry, Quaid-i-Azam University, Islamabad, Pakistan*

* *asheesgreat@yahoo.com*

NOVEL MECHANICALLY STABLE, HEAT RESISTANT AND NON-FLAMMABLE FUNCTIONALIZED POLYSTYRENE/EXPANDED GRAPHITE NANOCOMPOSITES

ABSTRACT

This study examined effect of inclusion of expanded graphite (Exp-G) on morphology, thermal, mechanical and flame retardant properties of PS, nitro-substituted polystyrene (N-PS) and amino-functional polystyrene (A-PS). FESEM showed exfoliated sheet morphology due to intercalation of N-PS and A-PS in expanded galleries. Tensile strength of A-PS materials (31.5-56.9 MPa) was higher than PS and N-PS. 10 % weight loss of A-PS nanocomposites (482-518 °C) was higher relative to pristine polymer and other nanocomposites. Cone calorimetry results revealed that there was lowering in PHHR of A-PS nanocomposites with 0.5 wt.% filler (428 kW/m²), while PS nanocomposites showed PHHR of 443 kW/m².

Key words: *Functional polystyrene; expanded graphite; dispersion; tensile strength; cone calorimetry*

INTRODUCTION

Preparation and properties of polymer/graphite composites has been focused by the researchers in recent decades [1-3]. Graphite is naturally abundant allotrope of carbon which is made almost entirely of carbon layers. In the layers, carbon atoms are bounded by Van der Waals forces and the absolute separation of graphite layers is difficult due to higher crystal lattice energy [4, 5]. Various methods have been explored for the preparation of hybrids with optimal physical properties and homogeneous dispersion of graphite particles in polymer matrix. In material science, various approaches for the fabrication of polymer/graphite composites have been developed and applied. The common methods include polymer blending with graphite or polymers intercalation into interlayer spacing of graphite [6-9]. Nano-dispersion of expanded graphite in various polymeric matrices such as poly(methyl methacrylate), polystyrene, and poly(vinyl chloride) using *in-situ* polymerization has been reported [10, 11]. The main aim of

these techniques is to attain uniform dispersion of graphite in continuous polymer matrix. Generally, it is difficult to achieve fine dispersion due to incompatibility of polymer and graphite. Therefore, it is essential to enhance the compatibility between nano-filler and polymer. Conventional polymer/graphite composites have been known to exhibit reduced physical properties due to poor dispersion ensuing deprived mechanical properties. Poor dispersion of filler may result in the aggregate formation owing to inadequate intercalation of macromolecules. The aggregates may not be able to reach closed cavities inside the expanded graphite. During processing, the graphite sheets around cavities tend to overlap each other and form accumulated mass. Polystyrene (PS) is a widely used polymer because of its good chemical resistance, low density, low cost, and ease of processing. However, high flammability and severe dripping during combustion greatly limit its application in buildings, transportation, and electrical appliances. In recent years, the development of halogen-free flame-retardant polymeric materials has been focused [12–14]. Traditional flame-retardant additives containing halogen elements are restricted nowadays and replaced by halogen-free counterparts such as phosphorus, metal hydroxides, nitrogen compounds, etc. Recently, carbon additives and nano-additives such as expanded graphite, graphite oxide, graphene, and carbon nanotubes are used in various polymeric systems to improve thermal and flame-retardant properties [15–19]. In addition, these nano-additives are important for improving the mechanical properties of original polymeric systems. Consequently, the previous research regarding the addition of graphite or functional graphite filler in polymers has focused the improvement of thermal stability, melt flow index, and non-flammability properties [20, 21]. The addition of graphite filler into polystyrene using melt blending technique is also the subject of research interest [22]. Though, the synergetic improvement of the thermal, non-flammable and tensile properties of polymer/graphite nanocomposites have been less explored. In this work, polystyrene has been modified into nitro-substituted polystyrene (N-PS) and amino-functional polystyrene (A-PS). Afterwards, the expanded graphite was prepared and reinforced in pure PS, N-PS and A-PS. Three series of polystyrene/expanded graphite nanocomposite were prepared using solution blending technique to achieve uniform dispersion of nano-sheets in the matrix. The structure, morphology, mechanical properties, thermal stability and flame retardancy of the nanocomposites were studied using appropriate techniques.

EXPERIMENTAL

Materials

Polystyrene (average $M_w \sim 350,000$, average $M_n \sim 170,000$), polyethylene glycol (average $M_w \sim 8,000$), graphite (fine powder), anhydrous tin(II)chloride (99 %) was procured from Aldrich and used as received. Sodium hydroxide (NaOH, 98 %), tetrahydrofuran (THF, 99 %), methanol (99 %), hydrochloric acid (HCl, 99 %), nitric acid (HNO_3 , 65 %) and sulfuric acid (H_2SO_4 , 98%) were supplied by Merck.

Instrumentation

Infrared (IR) spectra were recorded using Fourier transform infrared (FTIR) Spectrometer, Model No. FTSW 300 MX, manufactured by BIO-RAD, California, USA (4 cm^{-1} resolution). Field Emission Scanning Electron Microscopy (FE-SEM) of freeze fractured samples was performed using JSM5910, JEOL Japan. Thermal stability was verified by METTLER TOLEDO

TGA/SDTA 851 (California, USA) thermo gravimetric analyzer using Al_2O_3 crucible at a heating rate of $10\text{ }^\circ\text{C}/\text{min}$. Stress-strain behavior of the samples were studied using Testomeric materials testing machine M500–30CT. Test specimens were employed in the form of strips ($lwh\ 40\times 2\times 7 \pm 0.05\ \text{mm}^3$) according to ASTM D638 standard method. The crosshead speed was $2\ \text{mm}/\text{min}$ at room temperature. The data given are the average of three measurements. The combustion properties of pristine polymers and nanocomposites were calculated using cone calorimetry. Samples having dimensions $100 \times 100 \times 5\ \text{mm}^3$ were exposed to a FTT 0007 cone calorimeter (FTT Company, England) under a heat flux of $50\ \text{kW}/\text{m}^2$ according to ISO-5660 standard procedure.

Nitro-functionalization of polystyrene (N-PS)

The nitro-functionalization of polystyrene involved the dissolution of 10 g of polystyrene in 50 mL of THF with constant stirring of 3 h. Nitrating mixture (70 mL fuming HNO_3 and 30 mL concentrated H_2SO_4) was added drop wise to the stock solution. The mixture was cooled to $0\text{ }^\circ\text{C}$ in an ice bath for 6 h and then stirred at $60\text{ }^\circ\text{C}$ for 6 h. 30 % solution of NaOH was added to neutralize the mixture. The functionalized polymer obtained was dried at $80\text{ }^\circ\text{C}$ for 24 h.

Amino-functionalization of polystyrene (A-PS)

5 g of nitro-functionalized polystyrene was dissolved in 30 mL THF with constant stirring for 2 h. The reducing mixture was prepared by dissolving 60 g of anhydrous stannous chloride in 60 mL of hydrochloric acid at $60\text{ }^\circ\text{C}$ until the solution become clear. The polymer solution and the reducing mixture were mixed and refluxed at $80\text{ }^\circ\text{C}$ for 8 h. The mixture was neutralized with 30 % NaOH. The brown color polymer was obtained and dried at $80\text{ }^\circ\text{C}$ for 24 h.

Expansion of graphite (Exp-G)

Two-necked round bottom flask was charged with 150 mL of the mixture of HNO_3 and H_2SO_4 (1:2). 5 g of graphite was added to the above mixture and stirred for 12 h at room temperature. The mixture was neutralized with distilled water and then filtered. The powder was dried in an oven at $100\text{ }^\circ\text{C}$ for 12 h. For further expansion of the above modified graphite, the dried powder was placed in a heated muffle furnace at $500\text{ }^\circ\text{C}$ for 0.5 min. The temperature of $500\text{ }^\circ\text{C}$ was found adequate for thermal exfoliation. 1g of polyethylene glycol was dissolved in 30 mL of THF with sonication of 6 h. After that 2 g of expanded graphite was added to PEG and sonicated for 8 h. The mixture was neutralized and filtered. Finally the modified graphite was dried at $100\text{ }^\circ\text{C}$ for 12 h (Fig. 1) [23]. The sample designation, composition and codes used in this study are given in Table 1.

Preparation of nanocomposites from non-modified and modified polystyrene and expanded graphite

Three series of nanocomposites (PS 1-5, N-PS 1-5 and A-PS 1-5) were prepared with exfoliated graphite. Here again, 1g of polystyrene (PS, N-PS or A-PS), was dissolved in 10 mL of THF to prepare the stock solution with stirring of 6 h. Expanded graphite (0.01 g, 0.05 g, 0.1 g, 0.3 g and 0.5 g) was added to the stock solution and further stirred for 6 h. Thin nanocomposite films were cast in Teflon Petri dishes.

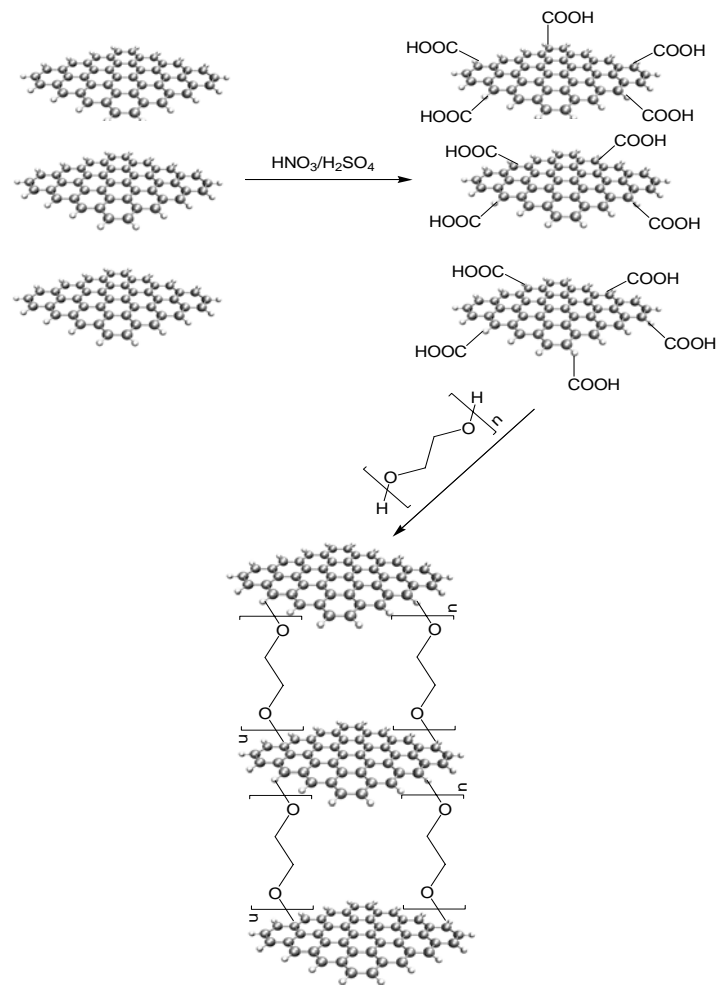


Fig. 1. Schematic illustration for the expansion of graphite using polyethylene glycol

Table 1. Sample codes and composition of the nanocomposites

Sample Code	Matrix	Expanded Graphite (wt. %)
PS 1	Polystyrene	0.01
PS 2	Polystyrene	0.05
PS 3	Polystyrene	0.1
PS 4	Polystyrene	0.3
PS 5	Polystyrene	0.5
N-PS 1	Nitro-functional polystyrene	0.01
N-PS 2	Nitro-functional polystyrene	0.05
N-PS 3	Nitro-functional polystyrene	0.1
N-PS 4	Nitro-functional polystyrene	0.3
N-PS 5	Nitro-functional polystyrene	0.5
A-PS 1	Amino-functional polystyrene	0.01
A-PS 2	Amino-functional polystyrene	0.05
A-PS 3	Amino-functional polystyrene	0.1
A-PS 4	Amino-functional polystyrene	0.3
A-PS 5	Amino-functional polystyrene	0.5

RESULTS AND DISCUSSION

FTIR analysis

Fig. 2 shows the FTIR spectra of N-PS 3 and A-PS 3 nanocomposites. The spectrum of N-PS 3 (Fig. 2A) displays strong vibration at 3025 and 3055 cm^{-1} due to aromatic C–H character. Moreover, the aliphatic C–H stretching vibrations at 2850 and 2921 cm^{-1} were present due to polystyrene structure.

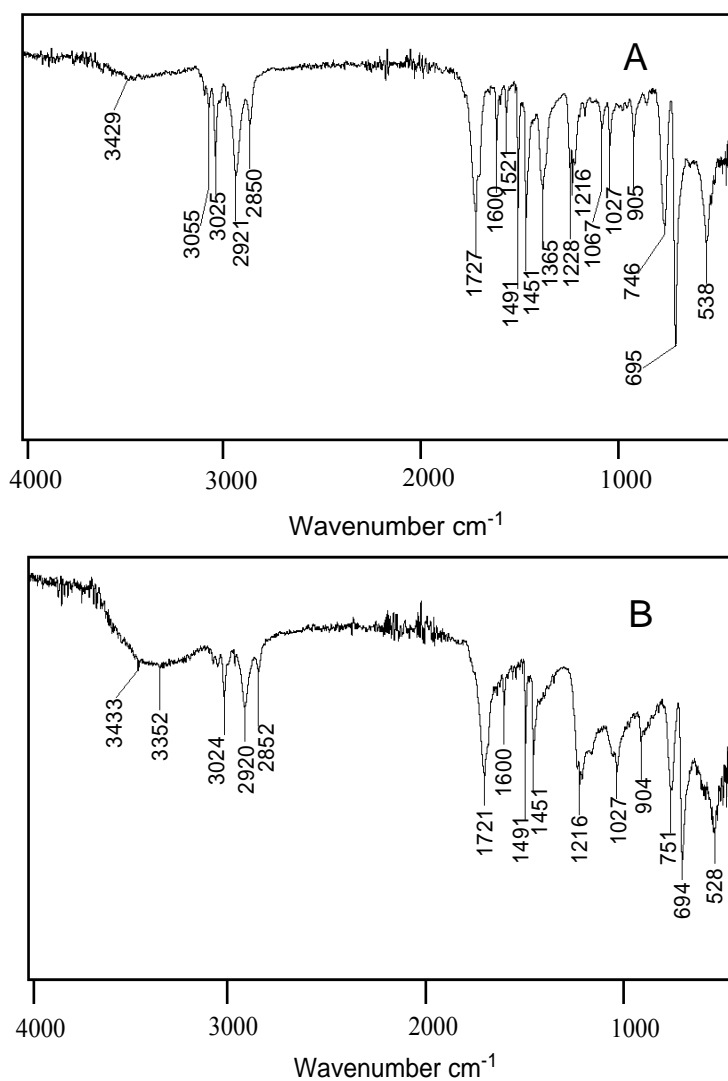


Fig. 2. FTIR spectra of (A) N-PS 3; and (B) A-PS 3 nanocomposites

The spectrum also exhibited O–H stretching vibration at 3429 due to the expanded graphite structure using PEG. A C=C peak (1600 cm^{-1}) corresponding to the sp^2 character was also appeared. The stretching vibration of C=O carbonyl groups introduced on the surface of expanded graphite appeared at 1721 cm^{-1} . Moreover, the asymmetric stretching vibration of NO_2 appeared at 1521 cm^{-1} indicating the successful attachment of NO_2 group to the matrix. The

stretching vibrations at 1216 and 1365 cm^{-1} were considered to be appear because of C–O–C and CO–H stretching. The C–H out of plane bending vibrations were found at 746 and 695 cm^{-1} related to benzene ring. FTIR spectrum of A-PS 3 is shown in Fig. 1B. The spectrum displayed O–H stretching vibration at 3433 due to the expanded graphite structure similar to the spectrum of N-PS 3. The N–H stretching vibration appeared at 3352 cm^{-1} signifying the attachment of amine group to the matrix, while NO_2 peak at 1521 cm^{-1} was disappeared. The aromatic C–H stretching vibration emerged at 3024 cm^{-1} while aliphatic C–H stretching vibration was observed at 2852 and 2920 cm^{-1} . The carbonyl stretch was also found at 1721 cm^{-1} . In A-PS 3 nanocomposite, C–O–C and C–H out of-plane benzene ring bending vibrations were also found at 1216, 751 and 694 cm^{-1} .

Mechanical properties

Table 2 presents the tensile properties of neat polystyrene, modified polystyrene, PS 1-5, N-PS 1-5 and A-PS 1-5 nanocomposites. Pure polystyrene, nitro-functional and amino-functional polystyrene depicted relatively lower tensile strength of 20.3, 22.6 and 25.7 MPa compared with nanocomposite series. The tensile modulus of these materials was also studied. The tensile modulus usually measures the resistance of a material to elastic/recoverable deformation under load. A stiff material has high modulus and undergoes slight change in shape under elastic loads while a flexible material has low modulus and changes its shape considerably.

Table 2. Mechanical properties of PS, N-PS, A-PS, PS 1-5, N-PS 1-5 and A-PS 1-5 films

Composition	Tensile Strength (MPa) \pm 0.04	Elongation at break \pm 0.01 (%)	Tensile Modulus (GPa) \pm 0.02	Toughness (Jm^{-3}) \pm 0.05
PS	20.3	0.02	0.7	0.14
N-PS	22.6	0.02	0.8	0.14
A-PS	25.7	0.02	0.9	0.15
PS 1	25.9	10.8	1.9	559
PS 2	31.3	9.4	2.7	622
PS 3	36.6	8.8	3.5	735
PS 4	38.9	7.8	5.3	844
PS 5	40.5	6.7	6.4	967
N-PS 1	29.7	12.3	3.3	654
N-PS 2	37.2	11.7	5.8	876
N-PS 3	43.1	10.2	7.1	889
N-PS 4	49.4	9.8	7.8	976
N-PS 5	52.3	8.2	8.4	1002
A-PS 1	31.5	14.1	6.2	798
A-PS 2	38.8	13.2	7.5	867
A-PS 3	46.2	12.7	8.8	1011
A-PS 4	52.8	11.4	9.7	1211
A-PS 5	56.9	10.2	10.1	1308

The tensile modulus PS, N-PS and A-PS was found to be lower 0.7, 0.8, 0.9 GPa relative to the composites. The most probable reason was that the inclusion of exfoliated graphite filler has probably increased the stiffness of material towards the applied load. On the other hand, the pristine and modified polymers without the nano-filler have relatively less rigid structure, which

was less resistant to the applied load. The toughness is the resistance to failure or crack propagation. Toughness relates to the amount of energy absorbed in order to propagate a crack. The materials with high toughness require greater energy to maintain the crack propagation. The toughness of PS, N-PS and A-PS was found to be 0.14, 0.14 and 0.15 Jm^{-3} .

While studying the effect of expanded graphite loading on the tensile strength, the PS 1-5 was found to have lower values in tensile strength (25.9-40.5 MPa) relative to N-PS 1-5 (29.7-52.3 MPa) and A-PS 1-5 (31.5-56.9 MPa) nanocomposites. The most probable reason was the increased toughness of the N-PS and A-PS matrices after modification and hybrid formation. However, the filler loading in the matrices (PS, N-PS and A-PS) resulted in higher mechanical stability compared with the pure polymers. The tensile modulus also had increasing trend in the nanocomposites.

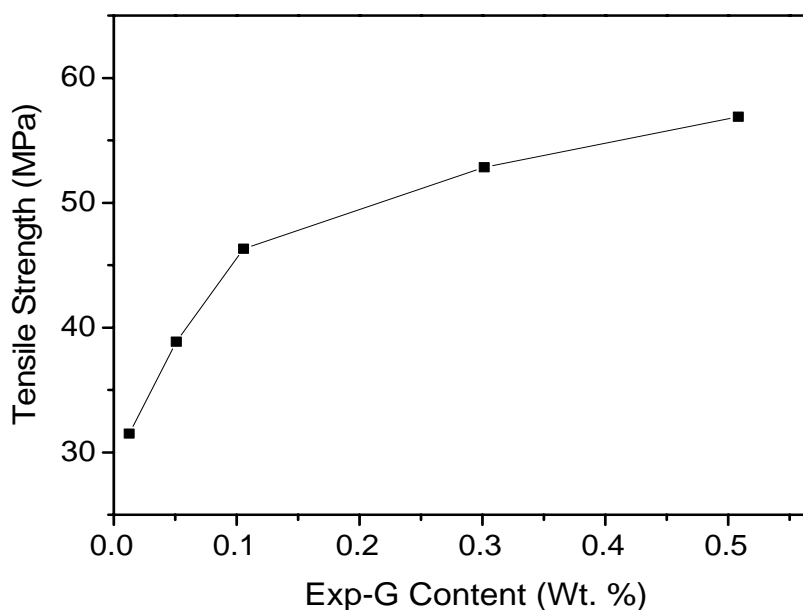


Fig. 3. Increasing trend of tensile strength vs. expanded graphite loading in APS-based nanocomposites

Here again, A-PS 1-5 showed higher values in the tensile modulus (6.2-10.1 GPa) relative to PS 1-5 (1.9-6.4 GPa) and N-PS 1-5 (3.3-8.4 GPa) nanocomposites. The toughness of the A-PS 1-5 nanocomposite series was also found to be higher 798-1308 Jm^{-3} relative to the PS 1-5 (559-967 MPa) and the N-PS 1-5 (654-1002 MPa). Dependence of the tensile strength of the N-PS 1-5 nanocomposites on expanded graphite content is given in Fig. 3. In the nanocomposite series prepared, the optimal results were obtained for 0.5 wt. % filler loading in amino-functionalized polystyrene matrix owing to the better intercalation of the functional polymer in expanded graphite galleries.

Morphological study

FE-SEM was performed for the samples including PS 5, N-PS 5 and A-PS 5. Fig. 4A-C shows the morphology of pure polystyrene matrix loaded with 0.05 wt. % expanded graphite. The surface morphology was observed to be of an encrusted structure reflecting its layered arrangement. However, the expansion of graphite sheets due to polymer intercalation was not so apparent in the micrographs because of the less interaction between the matrix and Exp-G.

The fractured surface of 0.05 wt. % expanded graphite loaded nitro-functional PS is given in Fig. 5A & B. The morphology of the samples was observed to be of a wrinkled and folded texture showing the layered microstructure. Fig. 5C-D also displayed wrinkled and folded consistency and the layering was more prominent in the A-PS matrix. The morphology of N-PS 2 and A-PS 2 also showed that the exfoliated graphite flakes tend to organize inside the polymer matrix owing to the fine dispersion. The folded and layered morphology is usually observed for the exfoliated graphite-based nanocomposites [24].

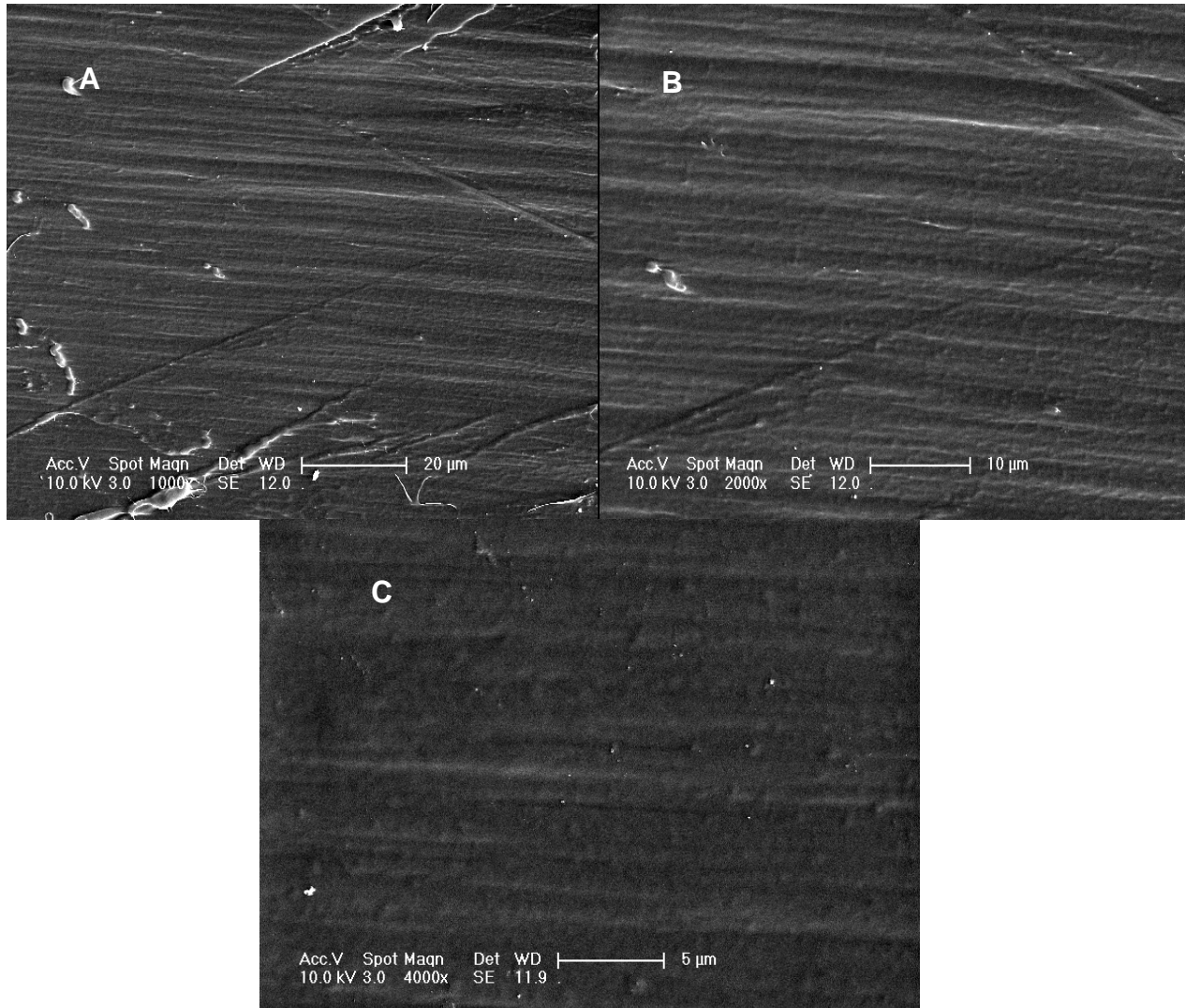


Fig. 4. FESEM micrographs of (A) PS 2 at 20 μm; (B) PS 2 at 10 μm; (C) PS 2 at 5 μm;

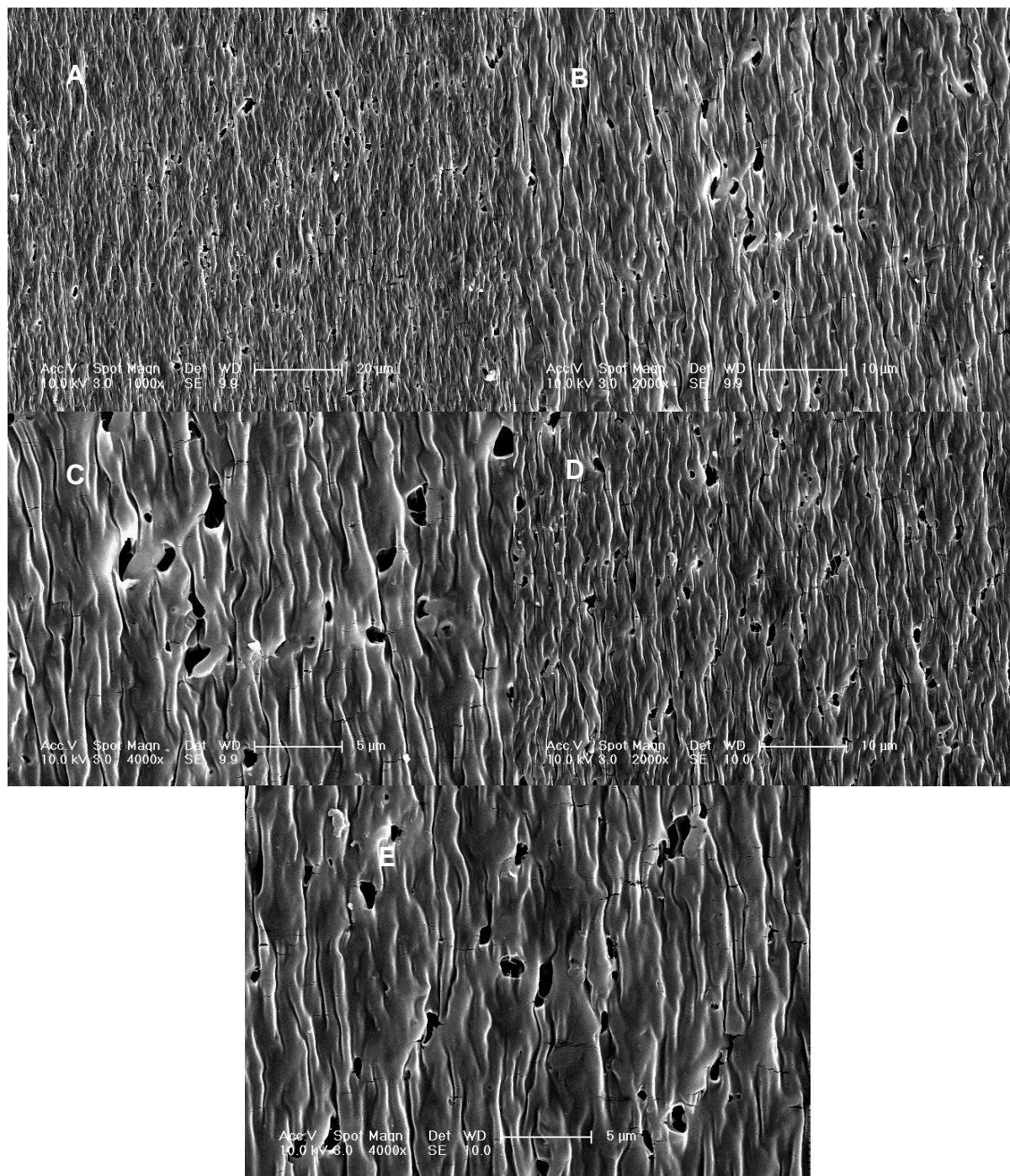


Fig. 5. FESEM micrographs of (A) N-PS 2 at 20 μm; (B) N-PS 2 at 10 μm; (C) N-PS 2 at 5 μm; (D) A-PS 2 at 10 μm; and (E) A-PS 2 at 5 μm

Thermal stability

The results for the PS, N-PS, A-PS, PS 1-5, N-PS 1-5 and A-PS 1-5 films are presented in Table 3. The data include the onset temperature of degradation (T_0), the temperature at which 10 % weight loss occurred (T_{10}), maximum weight loss temperature (T_{max}) and char yield. The T_0 of PS was 320 °C, while the T_0 values of the N-PS and A-PS were 345 and 370 °C respectively. For

the PS 1-5 series, the T_0 was 425, 431, 439, 446 and 459 °C for 0.01, 0.05, 0.1, 0.3 and 0.5 wt. % expanded graphite respectively. The T_{10} of PS 1-5 nanocomposite was also found to be higher than that of neat PS and the modified matrices as 432, 444, 450, 458 and 465 °C for 0.01, 0.05, 0.1, 0.3 and 0.5 wt. % loading. The T_{max} was 468, 470, 475, 483 and 492 °C for 0.01, 0.05, 0.1, 0.3 and 0.5 wt. % loading respectively in this series. For the neat N-PS loaded with 0.01-0.5 wt. % expanded filler, the T_0 , T_{10} and T_{max} was found to be in the range 425-459, 432-465 and 468-492 °C. Among the nanocomposites, the A-PS 1-5 provided the optimal thermal stability compared with the pure PS, N-PS and A-PS and the nanocomposites. The TGA curves for A-PS 1-5 nanocomposites are presented in Fig. 6. For the A-PS 1-5 series T_0 was 473, 481, 488, 492 and 501 °C for 0.01, 0.05, 0.1, 0.3 and 0.5 wt. % expanded graphite respectively. The T_{10} of A-PS 1-5 nanocomposite was also found to be higher than that of neat PS, the modified matrices, the nitro-functional matrix and its nanocomposite. The T_{10} was 482, 491, 498, 500 and 518 °C for 0.01, 0.05, 0.1, 0.3 and 0.5 wt. % loading respectively in A-PS 1-5 nanocomposite. T_{max} was 510, 517, 520, 529, and 534 °C for 0.01, 0.05, 0.1, 0.3 and 0.5 wt. % loading respectively in the A-PS-based nanocomposite.

Table 3. Thermal analyses data of PS, N-PS, A-PS, PS 1-5, N-PS 1-5 and A-PS 1-5 films

Composition	T_0 (°C)	T_{10} (°C)	T_{max} (°C)	Y_c at 600 °C (%)
PS	320	373	396	12
N-PS	345	382	402	26
A-PS	370	385	415	29
PS 1	425	432	468	44
PS 2	431	444	470	49
PS 3	439	450	475	50
PS 4	446	458	483	52
PS 5	459	465	492	54
N-PS 1	437	441	481	45
N-PS 2	445	449	484	51
N-PS 3	459	458	490	54
N-PS 4	462	465	494	55
N-PS 5	469	478	499	56
A-PS 1	473	482	510	57
A-PS 2	481	491	517	58
A-PS 3	488	498	520	60
A-PS 4	492	500	529	61
A-PS 5	501	518	534	63

T_0 : Initial decomposition temperature

T_{10} : Temperature for 10 % weight loss

T_{max} : Maximum decomposition temperature

Y_c : Char yield; weight of polymer remained

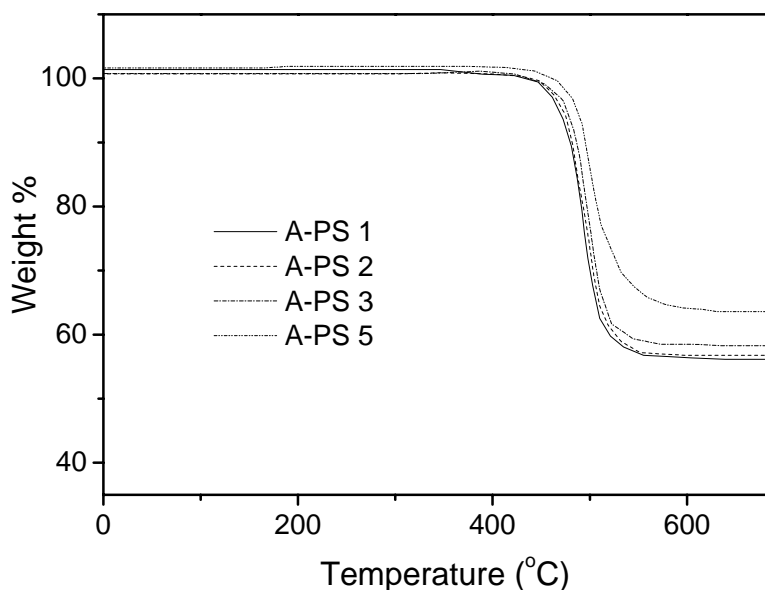


Fig. 6. Thermal degradation patterns of A-PS-based nanocomposites obtained through TGA

Above consequences have proved that the amino-modification of PS was beneficial for the enhancement of heat constancy of the nanocomposites. In the case of char residues at 600 °C, the char yield of expanded graphite-based nanocomposites was increased relative to that of the neat PS, N-PS, A-PS, N-PS 1-5 and A-PS 1-5 systems. The A-PS 1-5 nanocomposites depicted higher char yield values in the range of 57-63 % at 600 °C. The flame retardant properties of nanocomposites can also be studied in terms of the char yields. According to literature, the higher thermal residue in the range 600–700°C is often related to flame resistance [25, 26]. Moreover, the char yield up to 63 % shows that the polymers have high intrinsic fire resistance i.e. thermal stability. Increasing char formation could limit the production of combustible gases; decrease the exothermicity of the pyrolysis reaction and restrict the polymer's flammability. Furthermore the addition of expanded graphite in amino-functional matrix promoted the carbonization on the polymer surface, thus, increasing the heat resistance and contributed to the higher char residues. The flame retardancy of the materials was evaluated by cone calorimetric analysis.

Flame-retardant properties

To assess the flame retardancy, the heat release rate (HRR) and the peak heat release rate (PHRR) values are important parameters. The HRR plots for polystyrene and the nanocomposites are shown in Fig. 7. It was found that the nanocomposites had significantly lower HRR than that of the virgin polymer. The PHRR values of the PS, N-PS and A-PS were found to be higher 860, 844 and 823 kW/m² respectively (Table 4). The expanded graphite-based hybrids PS 5, N-PS 5 and A-PS 5 have considerably lower PHRR values as 443, 432 and 428 kW/m². The inclusion of expanded graphite to the PS matrix decreased the heat release values. The lower PHRR was obtained for the expanded graphite incorporated in amino-functional matrix. Pure polystyrene presented a sharp HRR owing to the degradation as well as the stabilization of the char formation [27]. The reduction of HRR values in A-PS 5 nanocomposite was also accompanied by the decrease in ignition time. The expanded graphite actually served as a barrier to mass transport and somewhat insulated the underlying polymer from the ignition.

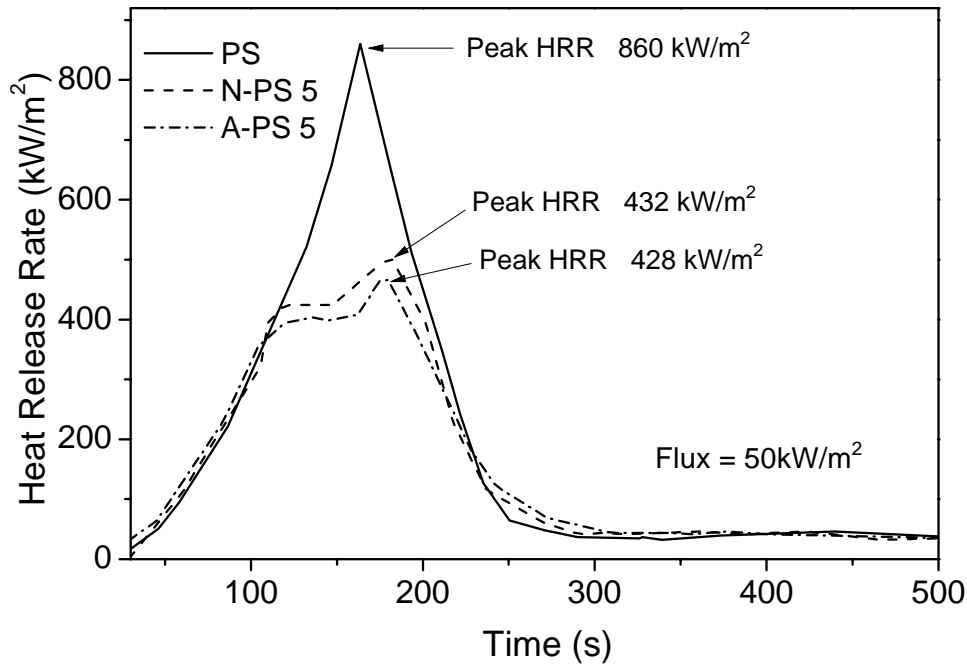


Fig. 7. Plots of heat release rate vs. burning time for PS and nanocomposites

Table 4. PHRR of pristine polymers and nanocomposites

Sample	PHRR (kW/m ²)
PS	860
N-PS	844
A-PS	823
PS 5	443
N-PS 5	432
A-PS 5	428

CONCLUSIONS

In this research effort, the expanded graphite was loaded in the neat polystyrene and functional polystyrene in different wt. %. The structural characterization by FTIR confirmed the structure of nanocomposites. The fracture toughness and the tensile strength of the nanocomposites were found to rise with Exp-G loading. The morphology analysis showed that the expanded graphite formed well-dispersed morphology in PS, N-PS and A-PS matrices. From TGA analysis, the thermal stability of the nanocomposites was found to increase with the increasing graphite content. The cone calorimetry results suggested the reduction in PHRR values with increasing filler content. The optimal flammability was obtained with the 0.5 wt. % expanded graphite, in this case the reduction in the peak PHRR was almost 50 % as compared to neat PS.

REFERENCES

1. Pluta M., Alexandre M., Blacher S., Dubois P., Jerome R.: Metallocene-catalyzed polymerization of ethylene in the presence of graphite, Structure and electrical properties of the composites, *Polymer* 42 (2001) 9293-9300.
2. Celzard A., Krzesinska M., Begin D., Mareche J. F., Puricelli S., Furdin G.: Preparation, electrical and elastic properties of new anisotropic expanded graphite-based composites. *Carbon* 40 (2002) 557-566.
3. Zheng W. G., Wong S. C., Sue H. J.: Transport behavior of PMMA/expanded graphite nanocomposites. *Polymer* 43 (2002) 6767-6773.
4. Chen G. H., Wu D. J., Weng W. G., Yan W. L.: Preparation of Polystyrene-Graphite Conducting Nanocomposites *via* Intercalation Polymerization. *Journal of Applied Polymer Science* 82 (2001) 2506-2513.
5. Uhl F. M., Wilkie C. A.: Polystyrene/graphite nanocomposites: effect on thermal stability. *Polymer Degradation and Stability* 76 (2002) 111-122.
6. Liu P. G., Gong K. C.: Synthesis and characterization of polyaniline intercalated graphite oxide composite. *Acta Polymerica Sinica* 4 (2000) 492-495.
7. Pan Y. X., Yu Z. Z., Ou Y. C., Feng Y. P.: Preparation and properties of nylon 6/graphite nanocomposite. *Acta Polymerica Sinica* 1 (2001) 42-47.
8. Xiao P., Xiao M., Liu P. G., Gong K. C.: Direct synthesis of a polyaniline-intercalated graphite oxide nanocomposite. *Carbon* 38 (2000) 626-628.
9. Chen G. H., Wu D. J., Weng W. G., Yan W. L.: Dispersion of graphite nanosheets in a polymer matrix and the conducting property of the nanocomposites. *Polymer Engineering and Science* 41 (2001) 2148-2154.
10. Panwar V., Kang B., Park J. O., Park S., Mehta R. M.: Study of dielectric properties of styrene-acrylonitrile-graphite sheets composites in low and high frequency region. *European Polymer Journal* 45 (2009) 1777-1784.
11. Stankovich S., Dikin D. A., Piner R. D., Kohlhaas K. A., Kleinhammes A., Jia Y., Wu Y., Nguyen S. T., Ruoff R. S.: Synthesis of graphene-based nanosheets via chemical reduction of exfoliated graphite oxide. *Carbon*, 45 (2007) 1558-1565.
12. Sudhakara P., Kannan P., Obireddy K., Rajulu A. V.: Flame retardant diglycidylphenylphosphate and diglycidyl ether of bisphenol-A resins containing Borassus fruit fiber composites. *Journal of Materials Science* 46 (2011) 5176-5183.
13. D. Konnicke, A. Kuhn, T. Mahrholz, M. Sinapius. 'Polymer nanocomposites based on epoxy resin and ATH as a new flame retardant for CFRP: preparation and thermal characterization. *Journal of Materials Science* 46 (2011) 7046-7055.
14. He Q. L., Song L., Hu Y., Zhou S.: Synergistic effects of polyhedral oligomeric silsesquioxane (POSS) and oligomeric bisphenyl A bis(diphenyl phosphate) (BDP) on thermal and flame retardant properties of polycarbonate. *Journal of Materials Science* 44 (2009) 1308-1316.
15. Murariu M., Dechief A. L., Bonnaud L., Paint Y., Gallos A., Fontaine G., Bourbigot S., Dubois P.: The production and properties of polylactide composites filled with expanded graphite. *Polymer Degradation and Stability* 95 (2010) 889-900.

16. Bian X. C., Tang J. H., Li Z. M., Lu Z. Y., Lu A.: Dependence of flame-retardant properties on density of expandable graphite filled rigid polyurethane foam. *Journal of Applied Polymer Science* 104 (2007) 3347-3355.
17. S. Peeterbroeck, F. Laoutid, J. M. Taulemesse, F. Monteverde, J. Lopez-Cuesta, J. B. Nagy, M. Alexandre, P. Dubois. Mechanical properties and flame-retardant behavior of ethylene vinyl acetate/high-density polyethylene coated carbon nanotube nanocomposites. *Advanced Functional Materials* 17 (2007) 2787-2791.
18. Isitman N. A., Kaynak C.: Nanoclay and carbon nanotubes as potential synergists of an organophosphorus flame-retardant in poly(methyl methacrylate). *Polymer Degradation and Stability* 95 (2010) 1523-1532.
19. Lee Y. C. R., Kim S. C., Lee H., Jeong H. M., Raghu A. V., Reddy K. R., Kim B. K.: Graphite oxides as effective fire retardants of epoxy resin. *Macromolecular Research* 19 (2011) 66-71.
20. Shi Y., Li L. J.: Chemically modified graphene: flame retardant or fuel for combustion. *Journal of Materials Chemistry* 21 (2011) 3277-3279.
21. Wang X., Song L., Yang H., Lu H., Hu Y.: Synergistic effect of graphene on antidripping and fire resistance of intumescent flame retardant poly(butylene succinate) composites. *Industrial & Engineering Chemistry Research* 50 (2011) 5376-5383.
22. Bao C. L., Guo Y., Yuan B., Hu Y., Song L.: Functionalized graphene oxide for fire safety applications of polymers: a combination of condensed phase flame retardant strategies. *Journal of Materials Chemistry* 22 (2012) 23057-23063.
23. Wen-Pin W., Cai-Yuan P.: Preparation and characterization of polystyrene/graphite composite prepared by cationic grafting polymerization. *Polymer* 45 (2004) 3987-3995.
24. Guo-Hua C., Da-Jun W., Wen-Gui W., Bin H., Wen-li Y.: Preparation of polystyrene-graphite conducting nanocomposites via intercalation polymerization. *Polymer International* 50 (2001) 980-985.
25. Kausar A., Zulfiqar S., Sarwar M. I.: An investigation on new high performance Schiff base polyurethanes. *High Performance Polymers* 24 (2012) 125-134.
26. Kausar A., Zulfiqar S., Sarwar M. I.: High performance segmented polyurethanes derived from a new aromatic diisocyanate and polyol. *Polymer Degradation and Stability* 98 (2012) 368-376.
27. Wang J. Q., Han Z. D.: The combustion behavior of polyacrylate ester/graphite oxide composites. *Polymer for Advance Technology* 17 (2006) 335-340.